AD-A082 552   HUGHES RESEARCH LABS   MALIBU CA   F/G 20/12
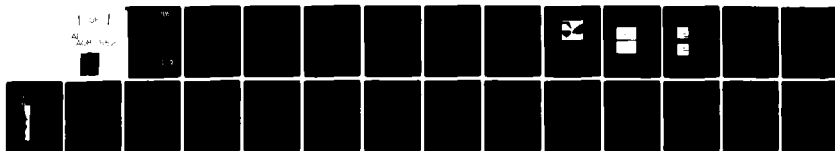   OPTICAL-MICROWAVE INTERACTIONS IN SEMICONDUCTOR DEVICES.(U)
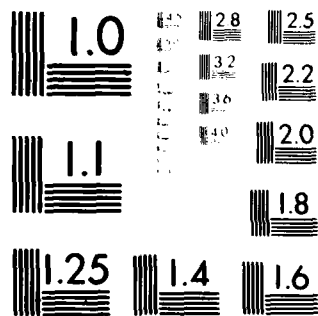   FEB 80 L FIGUEROA, C SLAYMAN, H W YEN   N00173-78-C-0192
UNCLASSIFIED   NL

END
DATE
FILMED
5-80
DTIC

(12) **LEVEL** II

(6) OPTICAL–MICROWAVE INTERACTIONS
IN SEMICONDUCTOR DEVICES

AD785 38

L. Figueroa, C. Slayman, and H.W. Yen

Hughes Research Laboratories
3011 Malibu Canyon Road
Malibu, CA 90265

(11) Feb 1980

(12) 26

DTIC
ELECTE
MAR 3 1 1980
S D
B

80 3 27 024

REPORT DOCUMENTATION PAGE		READ INSTRUCTIONS BEFORE COMPLETING FORM
1. REPORT NUMBER	2. GOVT ACCESSION NO.	3. RECIPIENT'S CATALOG NUMBER
4. TITLE (and Subtitle) OPTICAL-MICROWAVE INTERACTIONS IN SEMICONDUCTOR DEVICES		5. TYPE OF REPORT & PERIOD COVERED Quarterly Report 6 1 Oct. 1979 - 31 Dec 1979
		6. PERFORMING ORG. REPORT NUMBER
7. AUTHOR(s) L. Figueroa, C. Slayman, and H.W. Yen		8. CONTRACT OR GRANT NUMBER(s) N00173-78-C-0192
9. PERFORMING ORGANIZATION NAME AND ADDRESS Hughes Research Laboratories 3011 Malibu Canyon Road Malibu, CA 90265		10. PROGRAM ELEMENT, PROJECT, TASK AREA & WORK UNIT NUMBERS
11. CONTROLLING OFFICE NAME AND ADDRESS Defense Advanced Research Projects Agency 1400 Wilson Blvd. Arlington, VA 22201		12. REPORT DATE February 1980
		13. NUMBER OF PAGES 25
14. MONITORING AGENCY NAME & ADDRESS(if different from Controlling Office) Naval Research Laboratory 4555 Overlook Ave., S.W. Washington, DC 20375		15. SECURITY CLASS. (of this report) UNCLASSIFIED
		15a. DECLASSIFICATION DOWNGRADING SCHEDULE

16. DISTRIBUTION STATEMENT (of this Report)

Approved for public release; distribution unlimited.

17. DISTRIBUTION STATEMENT (of the abstract entered in Block 20, if different from Report)

18. SUPPLEMENTARY NOTES

19. KEY WORDS (Continue on reverse side if necessary and identify by block number)

GaAs FETs, GaAs FET detector, High-frequency response, Liquid phase epitaxial crystal growth, Optical waveguide, Photoconductivity, Traps.

20. ABSTRACT (Continue on reverse side if necessary and identify by block number)

GaAs FETs with built-in optical waveguides are being developed. The purpose is to allow optical signals to be coupled into the active region of the devices efficiently. These FETs will be useful for optical mixing, optical injection locking, and optical detection purposes.

DD FORM 1473 EDITION OF 1 NOV 65 IS OBSOLETE

We have designed, fabricated, and characterized a novel FET configuration. The structure consists of three layers: a GaAs active layer, a $Ga_{0.6}Al_{0.4}As$ waveguide layer, and a $Ga_{0.55}Al_{0.45}As$ buffer layer. The waveguide layer is made into a strip-loaded channel waveguide which serves as the input port for the optical signal. The guided optical signal leaks into the GaAs active layer once it reaches the FET mesa structure and is absorbed. The sensitivity and frequency response of the FET detector have been characterized. Our measurements indicate that the FET can respond to frequencies beyond 4 GHz with a sensitivity below that of a commercial PIN detector. The mode of operation for our detector appears to be photoconductivity. At dc, the sensitivity can be as high as 40 mA/mW. This large value probably indicates the presence of a large trap density.

ACCESSION for		
NTIS	White Section	☑
DDC	Buff Section	☐
UNANNOUNCED		☐
JUSTIFICATION		
BY		
DISTRIBUTION/AVAILABILITY CODES		
Dist:	AVAIL and/or	SPECIAL
A		

TABLE OF CONTENTS

LIST OF ILLUSTRATIONS

SECTION 1

INTRODUCTION AND SUMMARY

The ability to control the frequency and phase of solid-state microwave oscillators by optical injection of modulated light will allow optical fiber waveguides to replace heavy metallic waveguides in many microwave communication and radar applications. To achieve this will require microwave-modulated optical sources and a new class of microwave devices capable of interacting strongly with modulated optical signals.

The purpose of this study is to develop unique hybrid optical-microwave devices with optimal optical-microwave interaction characteristics. Specifically, we are developing GaAs FETs and GaAs Gunn diodes with built-in optical waveguides so that optical signals can be coupled to the active region of the device efficiently. The FETs will be used for optical mixing, optical injection locking, and optical detection purposes. The Gunn diodes will be used for high-speed pulse modulation of injection lasers.

During this quarter, we continued with the fabrication and characterization of GaAs waveguide FET detectors. The structure of these detectors consists of three layers: the GaAs top layer, the $Ga_{0.6}Al_{0.4}As$ waveguide layer, and the $Ga_{0.55}Al_{0.45}As$ buffer layer. The waveguide is made into a strip-loaded channel guide and serves as the input port for the optical signal. Once it reaches the FET mesa structure, the guided optical signal will leak into the GaAs layer and be absorbed. We have measured the dc and rf sensitivities, variation of rf drain-source current with drain source, and gate voltage. We have also compared the FET detector to a Si avalanche diode (APD) and calculated the dependence of detected current on device parameters. Our measurements indicate that the FET can respond to frequencies beyond 4 GHz with a sensitivity ~10 dB below that of an avalanche diode detector. At dc, the sensitivity can be as high as 40 mA/mW. That the sensitivity is so high probably indicates a large trap density.
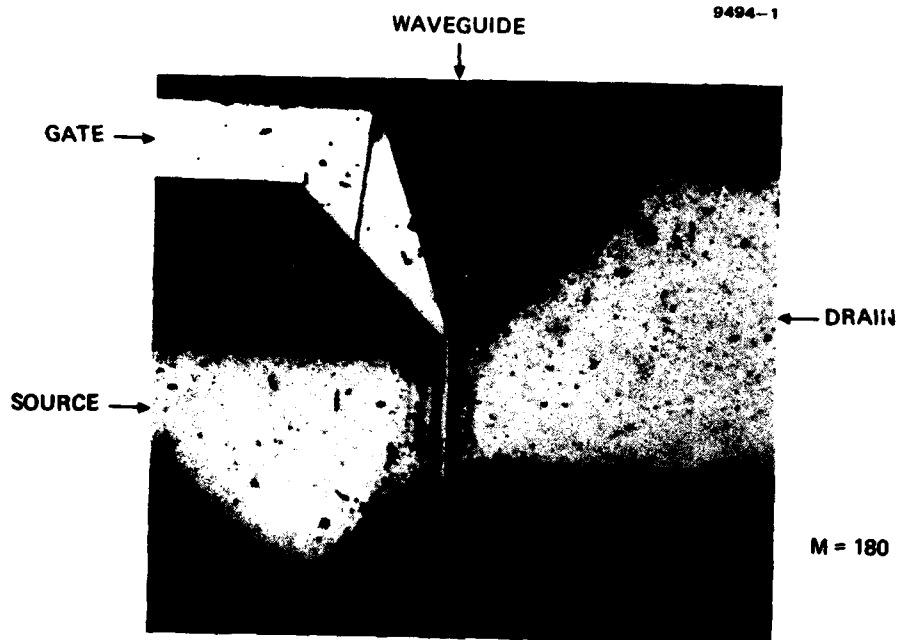
SECTION 2

DEVICE FABRICATION AND CHARACTERIZATION

In the last quarterly report, we described the fabrication process
for the FET detectors. We have continued using the same fabrication
procedure with the exception of the following changes. First, drain
source spacing was increased to 15 μm from 10 μm and active region
thickness was reduced to 0.2 μm from 0.5 μm. The first change was made
to simplify the processing and hence increase the yield of good devices.
The second change was made to produce devices with low pinchoff voltages
(i.e., V_p ~ 2 to 5 V). Figure 1 shows a top view and cross section of
the waveguide FET.

Figure 2 gives typical I_{DS}-V_{DS} characteristics. Figure 2(a) shows
I_{DS} versus V_{DS} for most of the devices from a wafer. The devices have a
peak I_{DS} of ~7 mA and a pinchoff voltage V_p of ~7 V. However, since our
Schottky gate breaks down at ~5 to 6 V, the devices cannot be completely
pinched off. Figure 2(b) shows the characteristics for some of the best
devices from the same wafer. In this case, $I_{DS} \approx 2.5$ mA and $V_p \approx 2.5$ to
3 V. We are almost able to pinch off the device. The incomplete pinch-
off is probably due to leakage current in the (GaAl)As layers.

We have measured the dc and rf optical sensitivities of the FET
detector. At dc, the sensitivity has a lower limit of ~4 to 12 mA/mW.
The large dc sensitivity is probably related to traps in the active
region or at the various interfaces. Typical drain-source character-
istics with and without illumination are shown in Figure 3. The rf
optical sensitivity is ~0.06 mA/mW at f = 1.1 GHz. The devices used in
this report were only sensitive to rf-modulated light when top illumina-
tion was used. Even though no rf optical response was observed from
the side, we did observe a large dc response. We do not yet fully
understand these observations. Three possibilities exist. First, the
thickness of the active region may be too thin to support an optical
mode since the waveguide is strongly asymmetric. Second, the lateral
confinement may be poor, which would cause the light to spread rapidly

(a) Top view
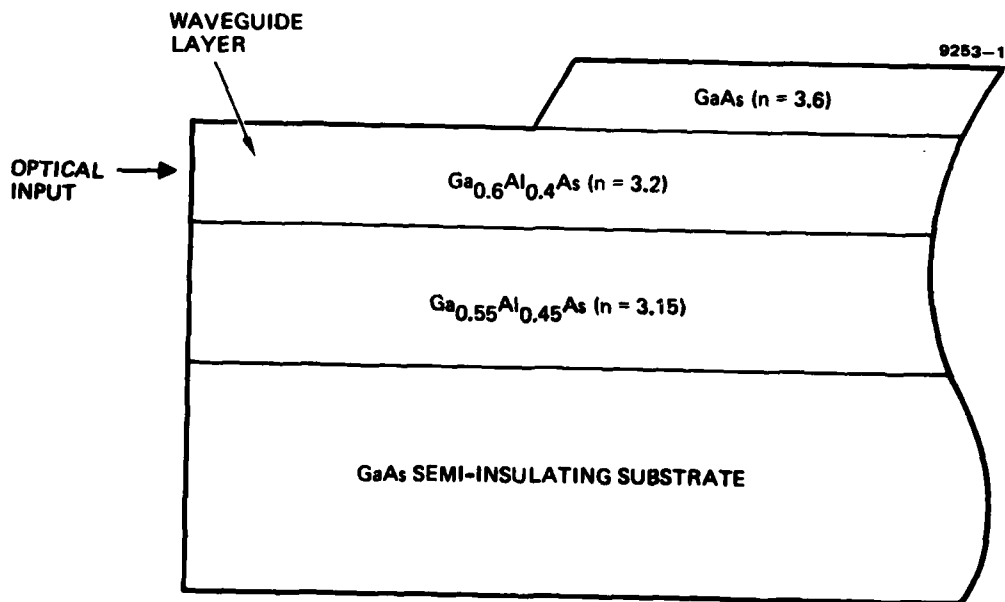
(b) Cross section
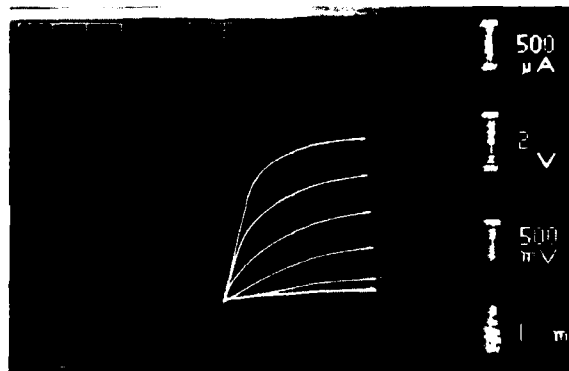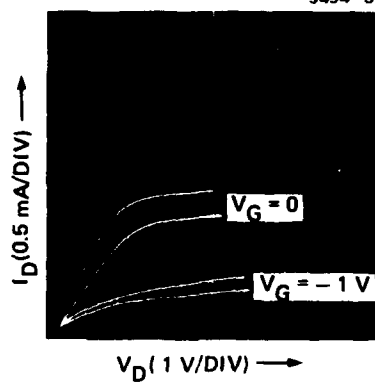
Figure 1. The FET waveguide detector.
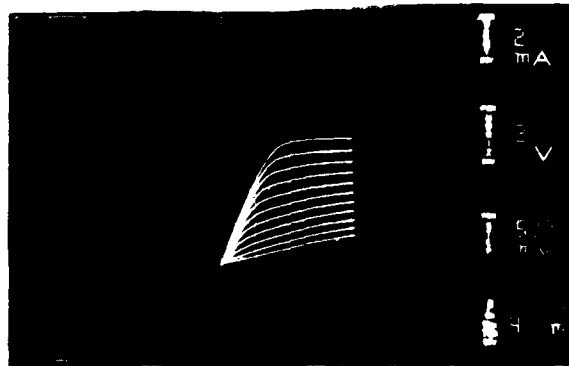
TYPICAL
CHARACTERISTIC

BEST DEVICES

Figure 2.   Drain-source current versus drain-source
            voltage.

9494-3

a) SIDE ILLUMINATION

I_D(0.5 mA/DIV)

$V_G = 0$

$V_G = -1\ V$

V_D(1 V/DIV)

b) TOP ILLUMINATION

I_D(0.5 mA/DIV)

$(V_G = 0)$

$(V_G = -1\ V)$

V_D(1 V/DIV)
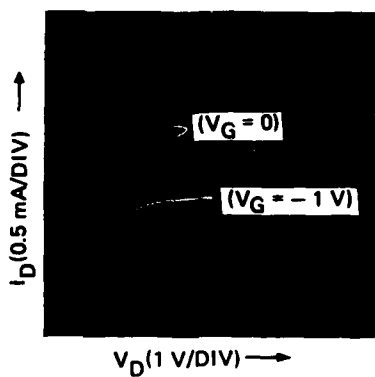
Figure 3.
Drain-source characteristics with
light injection.

9

in the lateral direction and prevent interaction with the high field region underneath the gate. And third, it is possible that, during the loading of the LPE boat, the Al concentrations were interchanged in the (GaAl)As layers and thus there is no waveguiding in the transverse direction. However, from the results in the last quarterly report, we know that the response of the FET is very similar in top and side illumination. Therefore, we feel the results presented here are representative of a working waveguide FET.

The rf response is shown in Figure 4(a), and the strip line circuit used is shown in Figure 4(b). The response is measured by biasing the injection laser at $I = 1.5 \ I_{th}$ and modulating the laser current. Figure 4(a) indicates a 3-dB cutoff frequency of ~1.35 GHz. Figure 4(a) also shows a resonance in the detected drain-source current at $f = 1.30$ GHz. This resonance has been observed in all the devices tested. We have speculated that this may be related to the strip-line circuit used. To check this, we changed the values of C_1 and C_2 (shown in Figure 4(b)). Initially, these capacitors were 0.1 nF. The values were changed to 10 nF. Figure 5 shows the new frequency response. Clearly, the resonance is absent and the response of the detector is flat up to 4 GHz, which is where the injection laser modulation depth has a resonance (relaxation oscillation) and then falls off. The cutoff frequency of the FET is associated with carrier recombination. Thus, carrier recombination can lead to a frequency response higher than 4 GHz. The frequency response and rf sensitivity are discussed in more detail below.

A measurement of the detected current ΔI_{DS} (f = 1.1 GHz) versus V_{DS} is shown in Figure 6. The curve shows three regions of operation. In region 1, the response is constant and corresponds to the velocity saturation. In regions 2 and 3, the detected signal decreases linearly (except at different slopes for regions 2 and 3) with decreasing V_{DS}.

The effects of gate bias on the detected currents are shown in Figures 7 and 8. Figure 7 is a plot of detected current ΔI_{DS} versus gate voltage V_G. The dashed curve results from a calculation (discussed in the next section) based on the equations describing an FET.

10

9494-4

C_1 0.1 nF   H – 50, ≠ 2

C_2 0 1 nF V_G = OPEN CKT.

                                V_{DS} = 4 V

V_{DS}, dB

f. GHz
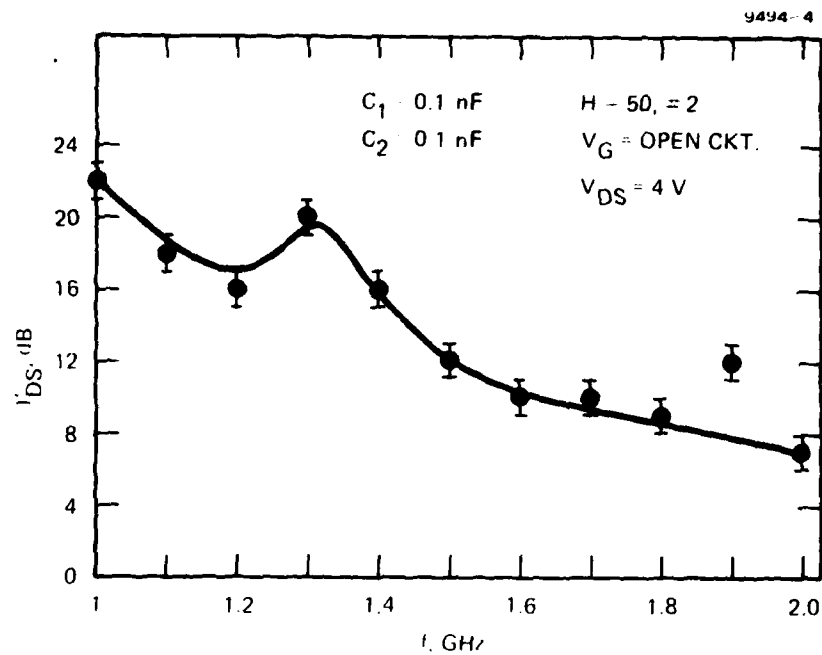
Figure 4(a).   Frequency response of FET detector.

9253-3

+V_{DD}

AMMETER

LIGHT

A

C_1 TO RF
SPECTRUM
ANALYZER

DRAIN

C_2 R_g

OPEN

GATE

SOURCE

-V_g
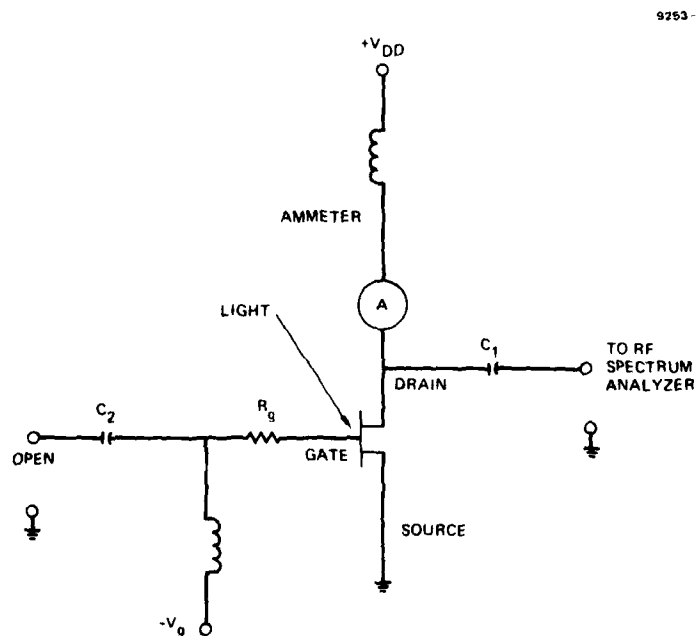
Figure 4(b).   Circuits used for characterizing
GaAs FET waveguide detector.

11

Figure 5. Frequency response of FET detector using a different stripline circuit.

15

Figure 6. Detected current $\Delta I'_{DS}$ (f = 1.1 GHz) versus drain source voltage V_{DS}.

Figure 7. Detected current ΔI_{DS} versus gate voltage V_G.

14

Figure 8. Detected current $\Delta I_{DS}'(f = 1.1 \text{ GHz})$ versus gate voltage V_G.

15

The agreement between theory and experiment is quite reasonable. It appears that a relatively large pinchoff voltage must be used if the agreement is to be good. The effect of rf optical modulation is shown in Figure 8, when negative bias on the gate increases. It is possible to obtain a 20-dB change in the rf drain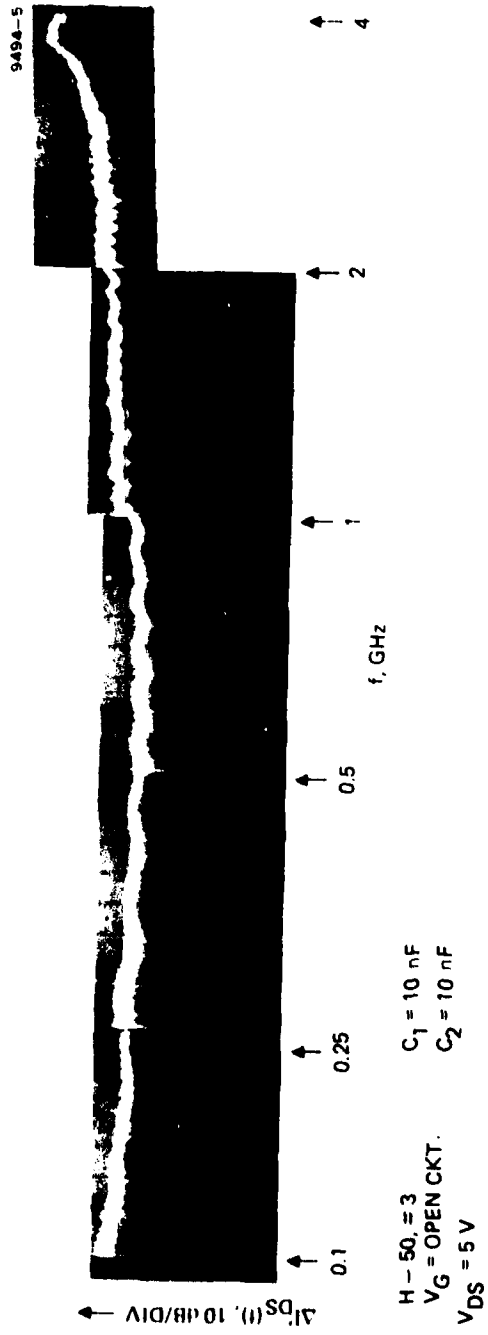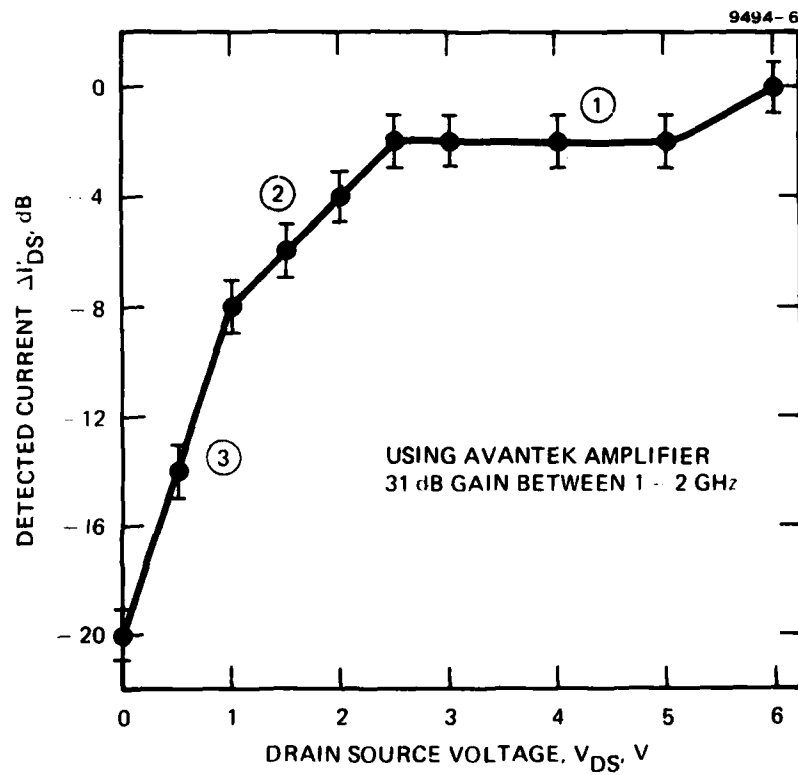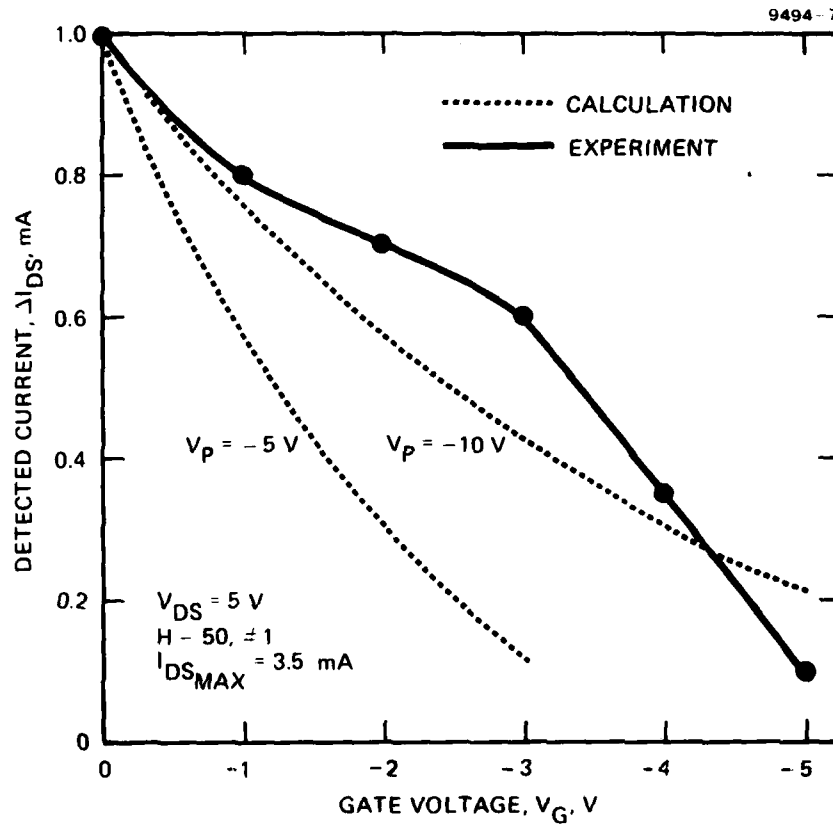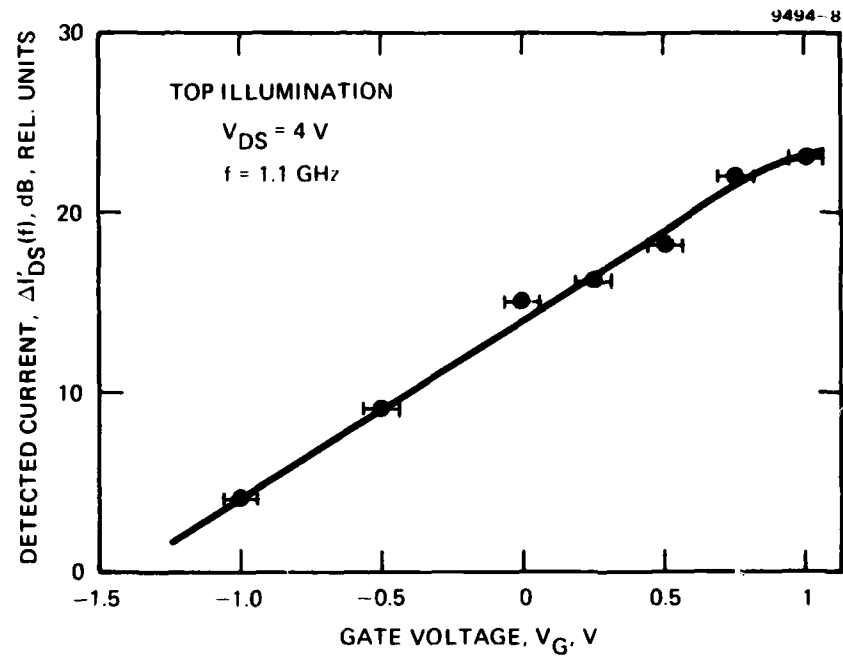-source current for a 2.5-V change in the gate voltage. Also note that the rate of change for the detected current with gate voltage is much larger at $f = 1.1$ GHz compared to dc. Furthermore, there is no significant change in the shape of the frequency response (except in the absolute value of detected $\Delta I'_{DS}$) as negative bias on the gate increases. Figure 9 shows measured detected gate current $\Delta I'_{Gs}$ ($f = 1.1$ GHz) as a function of gate voltage. The gate signal decreases as negative bias on the gate increases. No significant change in the cutoff frequency is observed. All the above results are consistent with a photoconductive mode of operation and do not show any photo-transistor action. Sugeta and Mizushima[1] recently observed that photo-transistor action is possible. However, our experiments do not seem to confirm this.

In Figure 10, the rf sensitivities of the FET and avalanche photo-detector (APD) (with the gain equal to 1) are compared. The rf sensitivity of the FET is 10 to 15 dB below the APD. However, there is no assurance that the two detectors collect the same amount of light. In fact, since the geometry of the FET is quite different (the gate metalization inter-feres with the incoming light and no AR coating is used), it is expected to collect less light than the APD.
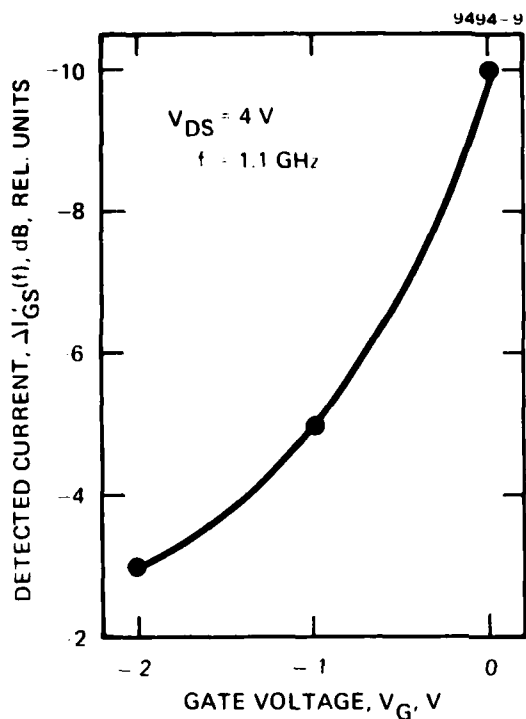
9494-9

Figure 9.
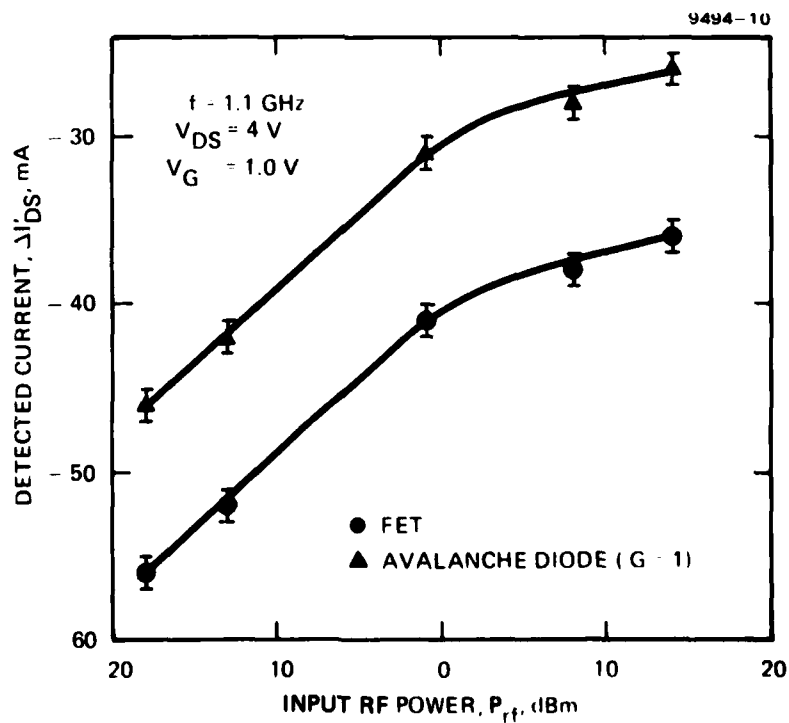Detected gate current $\Delta I'_{GS}$ (f = 1.1 GHz) versus gate voltage V_G.

9494-10

Figure 10. Comparison of FET and APD at GHz frequency (f = 1.1 GHz).

17

SECTION 3

CALCULATION OF THE DC AND RF SENSITIVITIES

The calculation of the sensitivity for a photoconductor has been given by DiDomenico and Svelto.[2] The change in photocurrent due to optical illumination is

$$\Delta I_o = \frac{\eta q \phi_o A \tau}{\tau_{tr}} \quad \text{at dc} \quad , \tag{1}$$

where $\phi_o A$ is the number of photons/sec (uniform illumination is assumed). The sensitivity can be written as

$$\frac{\Delta I_o}{\phi_o A \cdot h\nu} = S_o = \eta \left(\frac{\tau}{\tau_{tr}}\right) \frac{mA}{mW} \quad , \tag{2}$$

where η is the quantum efficiency, and we have assumed $h\nu$ (photon energy) $\simeq 1$ eV. The high-frequency response can be written as

$$\Delta I(f) = \eta q \phi_1 A \frac{\tau}{\tau_{tr}} \cdot \left(\frac{1}{1 + (\omega\tau)^2}\right)^{1/2} \quad , \tag{3}$$

where τ and τ_{tr} are the recombination and transit times of carriers, respectively. The 3-dB cutoff frequency is given by

$$f_{3dB} = \frac{1}{2\pi\tau} \quad . \tag{4}$$

The data in Figure 5 gives $f_{3dB} \simeq 4$ GHz. This leads to $\tau \leq 40$ psec. This value is different than the one we observed in the last report. The discrepancy was due to the measuring circuit, as we discussed previously in reference to Figures 4 and 5. The relatively small value for τ implies that the recombination is primarily due to the surface. Using the value given above for τ, the rf sensitivity can be calculated. First, the transit time of the device is calculated:

18

$$\tau_{tr} = \frac{L}{V_{sat}} , \tag{5}$$

where L is the drain-source spacing, and V_{sat} is the saturated velocity. We find $\tau_{tr} \simeq 173$ psec (assuming $\mu = 3000$ cm^2/V-sec and L = 15 μm). The rf sensitivity below the cutoff frequency is

$$\frac{\Delta I(f)}{\phi_1 \cdot A \cdot h\nu} = S_{rf} = \eta \left(\frac{\tau}{\tau_{tr}}\right). \tag{6}$$

Assuming a 30% quantum efficiency yields S_{rf} = 0.069 mA/mW. This would seem to imply that the FET detector is less sensitive than the PIN detector (or an APD with gain equal to 1). Using Figure 9, we find that the FET is 10 to 15 dB less sensitive than the APD (0.2 to 0.3 mA/mW) at f = 1.1 GHz. A factor of 10 less sensitivity could be partially explained by two factors. First, the quantum efficiency of the APD may be higher. For example, if η = 0.6 for the APD, the sensitivity would be $\sim$0.6 mA/mW, which is already 10 dB higher than the FET sensitivity. Second, it is difficult to know if the FET and APD collect the same amount of light. Since sensitivity is an absolute measurement, an error in the amount of light collected could lead to a large discrepancy in the measured sensitivity. If the FET is assumed to collect only 1/3 the light the APD collects, then the agreement between theory and experiment is narrowed. Thus, we feel the calculation agrees reasonably well with the experiment. Furthermore, it is clear that to increase the rf sensitivity of the device would require reducing the transit time of the FET. Our experimental results suggest that it is possible to obtain sensitivities of $\sim$0.6 mA/mW by decreasing the source-drain spacing to 1.5 μm. However, that value is quite optimistic since much less light would necessarily be collected at very narrow dimensions.

The last remaining problem is how to resolve the large dc response. We have observed that the dc sensitivity S_o ranges from a minimum of 4 to 12 mA/mW. The upper limit ranges from 14 to 42 mA/mW. These are very large numbers which need further clarification as to their origin. One possible explanation is to assume that there are hole-traps at the interface between the GaAs and (GaAl)As layers and at the surface of the active region. When electrons and holes are optically generated, the holes are quickly captured by the traps and then are very slowly re-emitted (governed by thermal generation). This effectively leads to a very long recombination time for the electrons. On the other hand, there must be a mechanism responsible for the high-frequency response. It appears that the traps cannot respond at the rf frequencies used. Thus, the effective rf lifetime of the traps must be relatively long compared to the operating frequency. The effective lifetime due to traps can be estimated using Eq. 2 with $\eta = 0.3$ and $S_o = 0.3 \ (\tau_{eff})/\tau_{tr} = 14$ to 42 mA/mW. This gives $\tau_{eff} \simeq 8$ to 24 nsec. This would lead to a 3-dB cutoff frequency f_{3dB} of 6.6 to 19.9 MHz. This implies a frequency response having two cutoff frequencies. Such a frequency response is schematically shown in Figure 11.
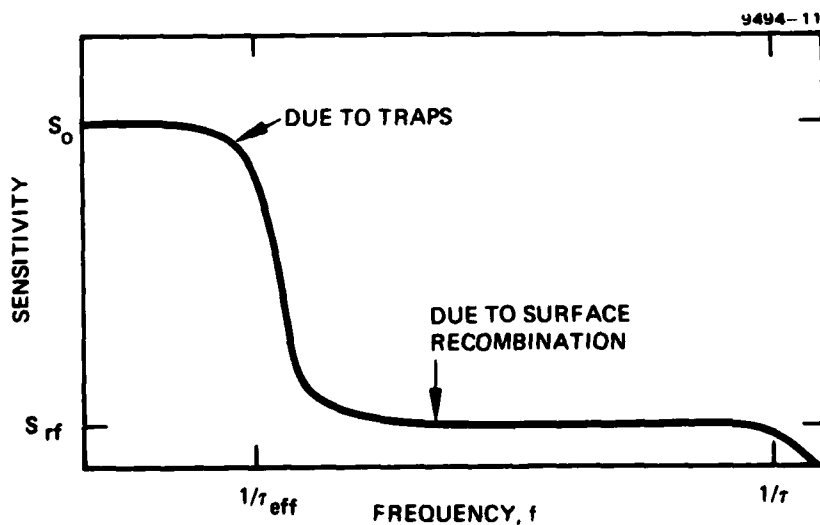

Figure 11. Schematic of total FET frequency response.

With respect to Figure 7, we discussed detected drain-source current ΔI_{DS} versus drain-source voltage V_{DS}. Next we discuss the calculation of such a curve. To calculate the effect of optical illumination on the characteristics of the FET, we begin with the expression given by Lehovec and Zuleog[3] for the drain-source current I_{DS}.

$$I_{DS} = \frac{e^2 N^2 d^3 \mu W}{6 \, \varepsilon \varepsilon_o L} \cdot \frac{3(u^2 - t^2) - 2(u^3 - t^3)}{1 + z(u^2 - t^2)} \, , \qquad (7)$$

where

N	is the carrier concentration in the channel
d	is the active region thickness
μ	is the electron mobility (N-type channel, low field)
W	is the device width
ε	is the relative dielectric constant
ε_o	is the dielectric constant in free space
L	is the gate length

$$z = \frac{\mu V_p}{V_m}$$

and

V_m	is the saturation velocity
V_p	is the pinchoff voltage.

The factor z takes into account the velocity-saturation effects in short-channel-length devices. In our calculations, we assume $z \simeq 0$. The other factors in Eq. 7, u and t, are defined as

$$u^2 = \frac{(V_{DS} - V_G - V_{Bi})}{V_p}$$

$$t^2 = - \frac{(V_G + V_{Bi})}{V_p} \, ,$$

where V_{Bi} is the built-in voltage. We should further note that Eq. 7 only applies for $u^2 < 1$. This condition is met when $I_{DS}(V_G)$ is maximum. For V_{DS} greater than needed to produce $I_{DS}(V_G)_{MAX}$, the equations are assumed to saturate.

When the FET is illuminated, carriers are generated in the active region. The generated carriers can be expressed as a function of the incident power P_{in} (for low light levels) by

$$\Delta N = \alpha' P_{in} \quad , \tag{8}$$

where α' is a constant that depends on the geometry of excitation and the lifetime of the injected carriers. With optical illumination present, the background carrier density changes to $N + \Delta N$, and the detector current becomes $I_{DS} + \Delta I_{DS}$. Eq. 7 can then be written as

$$I'_{DS} = Kf(u,t)(N + \Delta N)^2 \quad , \tag{9}$$

where I'_{DS} is with optical illumination

$$K = \frac{e^2 d^3 W \mu}{6 \varepsilon \varepsilon_o L}$$

$$f(u,t) = 3(u^2 - t^2) - 2(u^3 - t^3) \quad .$$

If low-level injection is assumed, then ΔN will be much smaller than N, and $(N + \Delta N)^2$ can be written as

$$(N + \Delta N)^2 \simeq N^2 + 2N\Delta N \quad . \tag{10}$$

The photocurrent ΔI_{DS} is given by

$$\Delta I_{DS} = 2KN\Delta N \, f(u,t) \quad . \tag{11}$$

Eq. 11 can be rewritten as

$$\Delta I_{DS} = \frac{2 I_p V_p}{N} \alpha' P_{in} [f(u,t)] \tag{12}$$

22

where we have used:

$$I_p = \frac{ed\ N\ \mu W}{3L} \qquad \text{(the maximum channel current)}$$

$$V_p = \frac{eNd^2}{2\varepsilon\varepsilon_o} \qquad \text{(the pinchoff voltage.)}$$

Eq. 12 can be plotted as a function of gate voltage and compared to experiment. In Figure 7, ΔI_{DS} is plotted versus gate voltage. The bracketed portion in Eq. 12 is fitted to the point $V_G = 0$. In the figure, plots have been made for two values of pinchoff voltage: $V_p = 5$ and 10 V. The lower value is probably closest to the actual device value. However, it does not fit the experimental results very well. The discrepancy between calculated and experimental results is not yet well understood. One known possibility exists for the discrepancy. We have assumed that the generated carriers are independent of device parameters. However, a large gate voltage could affect the number of carriers that reach the drain. Thus, this effect should be included in our formulation.

SECTION 4

PLANS FOR THE NEXT QUARTER

During the additional quarter we will resume the short optical pulse generation study. Up to now in the program we have generated optical pulses less than 150 ps wide at a few gigahertz repetition rates. However, we have not determined the ultimate limits of the injection laser mode-locking approach. Problems such as the shortest pulse width and the highest repetion rate achievable, the pulse shape, and the pulse stability will be studied.

REFERENCES

1. T. Sugeta and Y. Mizushima, Jap. J. Appl. Phys. $\underline{19}$, L27 (1980).

2. M. DiDomenico, Jr. and O. Svelto, Proceedings IEEE $\underline{52}$, 136 (1964).

3. K. Lehovec and R. Zuleeg, Solid State Electron. $\underline{13}$, 1415 (1970).